Journal of Materials Chemistry A

A Solid Electrolyte Interphase to Protect the Sulfurized Polyacrylonitrile (SPAN) Composite for Li-S Batteries: Computational Approach Addressing the Electrolyte/SPAN Interfacial Reactivity

Journal:	*Journal of Materials Chemistry A*
Manuscript ID	TA-ART-01-2021-000110.R1
Article Type:	Paper
Date Submitted by the Author:	21-Feb-2021
Complete List of Authors:	Perez-Beltran, Saul; Texas AandM University, Chemical Engineering Balbuena, Perla; Texas AandM University, Chemical Engineering

A Solid Electrolyte Interphase to Protect the Sulfurized Polyacrylonitrile (SPAN) Composite for Li-S Batteries: Computational Approach Addressing the Electrolyte/SPAN Interfacial Reactivity

Saul Perez Beltran[1], and Perla B. Balbuena[1,2,3],*

[1]Department of Chemical Engineering,[2] Department of Materials Science and Engineering, and [3]Department of Chemistry, Texas A&M University, College Station, Texas 77843, United States

*e-mail: balbuena@tamu.edu

Abstract

This study addresses the reactivity of multiple solvents and lithium bis(fluorosulfonyl)imide (LiFSI) at the interface with sulfurized polyacrylonitrile (SPAN) in multiple stages of lithiation via *ab initio* molecular dynamics simulations. Both ether 1,3-dioxolane (DOL) and dimethyl carbonate (DMC) proved stable on the lithiated SPAN surface regardless of the lithium content, meaning that neither of these species likely contributes to growing a solid electrolyte interphase (SEI) coating to protect the SPAN composite. Conversely, cyclic carbonates ethylene carbonate (EC) and fluoroethylene carbonate (FEC) show to be very active. The EC reduction occurs only on a highly lithiated surface with a 3.0 Li/S molar ratio, the equivalent of the SPAN composite in an over-discharge regime with voltages close to 0.0 V vs. Li/Li^+. The FEC reduction starts with a 2.0 Li/S molar ratio and above, suggesting that FEC could act as a useful additive in electrolyte formulations with EC. Both EC and FEC follow multiple reduction mechanisms to produce complex reduction products and LiF in the FEC case. We provide a mechanistic description for each detected decomposition path. The LiFSI salt also proves reactive against the lithiated SPAN surface. The FSI^- defluorination is the dominant reduction path. However, the $SO_2NSO_2F^-$ and $SO_2NSO_2^{2-}$ species proved stable against S-N cleavage. This behavior makes the LiFSI salt a potential candidate for SPAN-based Li-S batteries because it produces LiF without releasing SO_2.

Introduction

The lithium-sulfur (Li-S) electrochemical system is an attractive low-cost alternative for long-range electric vehicles because it delivers high theoretical energy density (2600 Wh/kg) and enjoys widespread availability of raw materials.[1-3] The task before the commercialization of this energy storage system relies on enhancing the sulfur's low electronic conductivity, stabilizing the highly reactive lithium metal anode, and improving the battery's rapid capacity fading. However, this enterprise proves challenging due to the interconnected nature of the battery; any

modification/improvement on either electrode or the electrolyte directly affects the other components of the battery.[4]

Recent studies show that the sulfurized polyacrylonitrile (SPAN) composite improves sulfur's cathode electrochemical performance.[5-10] The graphitized carbonaceous structure provides extended electronic pathways and hinders lithium polysulfides' dissolution (LiPSs). The covalent interactions between the graphitized backbone and the sulfur chains hanging around it induce a solid-solid lithiation mechanism that avoids the formation of soluble long-chain lithium polysulfides. However, it is noticed that regardless of these electrochemical advantages, the SPAN-based battery's performance still depends largely on the electrolyte formulation. The SPAN composite shows stable cycling with carbonate-based electrolytes but not with ether-based electrolytes, while the lithium metal anode behaves otherwise.[8, 11]

The above observation shows that the interfacial electrode/electrolyte's behavior determines much of the electrodes' performance. Understanding the decomposition mechanism of the electrolyte molecules on the electrode surface and the correct tuning of its self-limiting nature is crucial to take advantage of this inevitable process to direct it towards the engineering of a passivation coating – so-called solid electrolyte interphase (SEI) – able to protect the electrode against polysulfides dissolution, limit the uncontrolled electrolyte decomposition, and extend the battery lifespan. Recently, the research interest focuses on testing electrolyte formulations to grow SEI coatings on both electrodes simultaneously. A bilateral SEI layer offers higher Coulombic efficiency and prevents polysulfide dissolution and dendrite growth.[11, 12] So far, the electrolyte formulations based on carbonate/ether solvent mixtures have proven more effective in this enterprise. For example, scanning electron microscopy (SEM) imaging performed on lithium metal anodes and SPAN-based cathodes shows the growth of smooth and robust passivation layers on both electrodes if using a 1 M lithium bis(trifluoromethane sulfonyl) imide (LiTFSI) salt dissolved in a solvent mixture made of ethylene carbonate (EC), dimethyl carbonate (DMC), and 1,3-dioxolane (DOL), as the electrolyte.[11] Moreover, this battery system's electrochemical testing indicates enhanced battery performance, even with low electrolyte/sulfur ratios, crucial for practical applications.

This study evaluates the reactivity of multiple solvents and a lithium salt against lithiated SPAN surfaces via *ab initio* molecular dynamics (AIMD) simulations. The formation of a protective coating on cathode electrodes is viable in SPAN-based Li-S batteries at low voltages close to the end of discharge during the first discharge,[13, 14] which correlates with the irreversible capacity loss between the first two cycles for this type of electrochemical system.[8] The solvents

of choice in this work are DOL, DMC, EC, and fluoroethylene carbonate (FEC), and the lithium salt is lithium bis(fluorosulfonyl)imide (LiFSI). The ether DOL solvent is the preferred choice in conventional Li-S batteries because of its stability against the lithium metal anode and its ability to solubilize LiPSs to increase the cathode's wettability.[8, 11, 15, 16] However, experiments show that this solubilization ability threatens the SPAN composite's cycling stability.[8] Understanding its interaction with the lithiated SPAN composite is critical to elucidate its practical use for growing useful bilateral SEI layers. Carbonate-based electrolytes show improved performance with SPAN-based Li-S batteries.[6, 8] The linear carbonate ester DMC has proven useful to lower the electrolyte's viscosity. Among linear carbonates, the DMC-based electrolytes produce the highest discharge capacity after repeated cycling.[17] The cyclic carbonate ester solvent EC is of traditional use in Li-ion batteries; hence its implementation with SPAN-based batteries represents a shortcut to this technology's faster commercialization. The fluorinated FEC solvent reportedly produces a robust and elastic LiF-rich SEI layer on lithium metal anodes, Li_xSi_y allows, and S/C composites. [12, 18-21] Alongside EC, the FEC solvent is a low-cost coating-forming carbonate solvent that enjoys widespread use in conventional Li-ion batteries.[14, 21-23] LiF components strengthen the SEI layer with fast Li^+ transport properties that improve safety and provide a longer cycle life.[21, 24] Besides, the FEC possesses a low/high melting/flash point and a low solubility of LiPSs.[18] Finally, the LiFSI salt calls researchers' attention due to its high solubility in many organic solvents and its ability to form LiF-rich SEI layers.[25] Moreover, compared to the LiTFSI salt, commonly used in rechargeable Li-ion batteries, the LiFSI salt offers lower solubility of LiPSs and inhibits electrolytic corrosion.[4, 26]

Computational Methods

We explore the SPAN/electrolyte interface behavior via AIMD simulations performed with the Vienna ab initio simulation package (VASP – version 5.44). [27-29] The time step is one fs, the Nose thermostat controls the temperature at 330 K,[30, 31] and the integration of the equations of motion is performed with the Verlet algorithm. The cutoff for the plane-wave basis set dealing with valence electrons is 400 eV. Furthermore, the projector wave potential (PAW) method treats the core-electron dynamics.[32] The Perdew-Burke-Ernzerhof gradient approximation (PBE-GGA) addresses the exchange-correlation functional,[33] and the Monkhorst-Pack grid method set to 1x1x1 integrates the Brillouin zone.[34] The convergence criterion for the self-consistent electronic loop is 10^{-4} eV, while the ionic relaxation break condition is 10^{-3} eV. The approximation for partial occupancies is used with the Gaussian smearing method adjusted to 0.05 eV. We apply the van der Waals correction using the DFT-D3 method to ensure an

adequate description of dispersion forces.[35-38] Each AIMD run lasts 10 picoseconds (ps) for the bulk electrolyte calculations and 20 ps for SPAN/electrolyte interface configurations. In some cases, we perform DFT geometry optimizations on selected configurations. For these calculations we use the same simulation parameters used in AIMD but with the ionic convergence criterion set to 0.02 eV/Å and the ionic positions are updated with the conjugate gradient algorithm.

To identify radical species we perform a spin-polarized single-point energy calculation to calculate the projected density of states (pDOS) with the software package local orbital suite toward electronic-structure reconstruction (LOBSTER).[39, 40] We use the Bunge's description for the local basis functions needed for the projection calculations with the 1s orbital for hydrogen, 2s for lithium, 2s and 2p for carbon, nitrogen, and oxygen, and the 3s and 2p for sulfur. The absolute charge spilling is lower than 1.75% in all cases. Finally, the calculation of electronic charges is carried out with the grid-based Bader method developed by Henkelman and coworkers.[41]

Bulk Liquid Calculations

Pure Solvents

Table 1 outlines the solvents used in this work. We first pack the solvent molecules to the listed bulk density in a cubic simulation cell of length 12.5 Å along each coordinate and run a ten ps AIMD simulation to let the solvent molecules reorient in space before settling into an equilibrated configuration at 330K. This calculation creates a baseline to check for changes in the molecules' electrolyte charge distribution between the bulk electrolyte and regions close to the SPAN surface. A packing procedure randomly places the solvent molecules in the empty space, and is followed by a geometry optimization using the universal force field with the steepest descent algorithm as implemented in the Materials Studio software (version 8) to eliminate possible too-near atom-atom interactions. Before packing, we optimize the individual solvent molecules within a 12.5 Å x 12.5 Å x 12.5 Å cubic unit cell. We do not study mixtures of solvents in this work, even though a typical electrolyte formulation is a mixture of multiple solvents and additives.[11] Earlier calculations of the reactivity of mixtures of solvents on a lithium metal anode proved that the use of solvent mixtures does not affect each species' overall stability relative to the pure formulation.[16]

Table 1: Solvent Formulations used in this work

Electrolyte Formulation	Density [g/cm^3]	# Packed Molecules
Pure Solvents		
DOL	1.06	17
EC	1.32	18
FEC	1.41	16
DMC	1.07	14

Figure 1 depicts the solvent molecules with their respective atomic labeling and charge distribution averaged in the liquid phase. For the DOL molecules, the largest partial charges are on the oxygen O_2 atoms and the C_1 carbon. As a pure solvent, this molecule's average charge is 0.0002 |e| with -1.017 |e| and 0.832 |e| cumulated on the O_2 and C_1 atoms. For the EC solvent, the largest partial charges are on the O_1 (-1.13 |e|) and C_1 atoms (2.05 |e|), whereas the total averaged cumulated charge is -5x10^{-6} |e|. The large charge difference between the O_1 and C_1 atoms agrees with the large dipole moment reported for this molecule.[22] Meanwhile, the electronic charge on the O_1 and C_1 atoms in the FEC molecule are -1.11 |e| and 2.03 |e|, respectively, similar to the EC molecule but with a significant charge concentration on the F atom (-0.62 |e|). However, this electron accumulation on the F atom does not change the molecule's total electronic charge as it remains neutral. Earlier reports indicate that this "electron-withdrawing" effect on the F atom leads to a lower freezing point, lower viscosity, and higher oxidative stability, as well as improved wettability toward the electrode and separator,[21] key for practical applications that require low electrolyte/electrode ratios.[11]

For the DMC molecule, the charge difference between the O_1 and C_1 atoms is 3.18 |e|, proper of carbonate ester solvents. This set of calculations with DMC shows that this molecule settles only in its trans-trans conformation with C_{2v} symmetry.[42] Later calculations with the LiFSI salt shows that the trans-cis conformation with C_s symmetry also exists if the molecule engages in a solvated structure with the Li^+ ion. However, we found out that this symmetry change does not influence the molecule's reductive stability against lithiated SPAN structures.

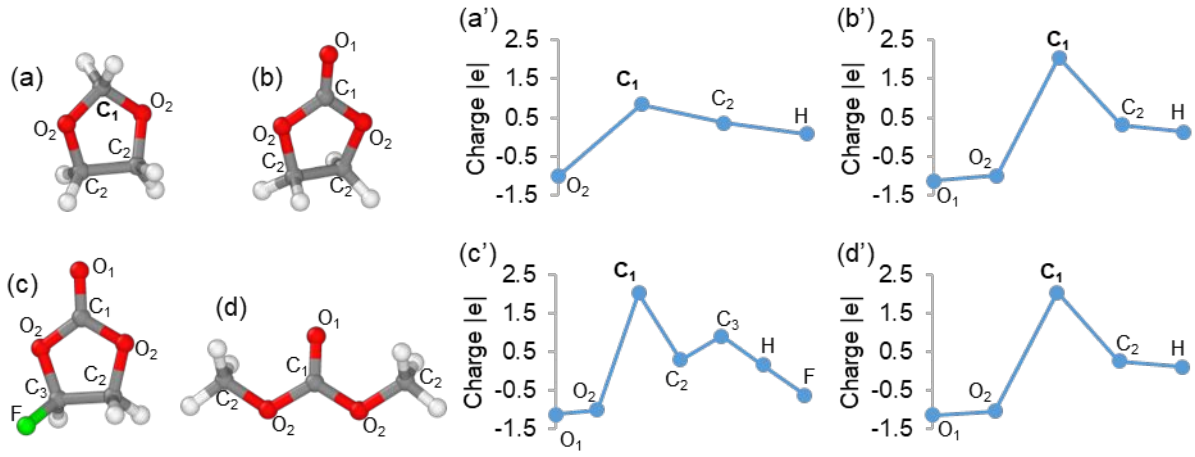

Figure 1: Solvent molecules and average electron charge distribution in liquid phase: (a) and (a') DOL solvent, (b) and (b') EC, (c) and (c') FEC, (d) and (d') DMC. Oxygen atoms are the red spheres, carbon atoms the gray ones, fluorine is in green, and hydrogen white.

LiFSI/Solvent Mixtures

LiFSI is a salt candidate compatible with SPAN-based Li-S batteries that can grow high-quality LiF coatings on cathode and anode surfaces.[4, 12] Ionic liquid (IL) formulations with FSI^- anions possess low viscosity and outstanding chemical stability. Besides, the FSI^- inhibits the current collector electrolytic corrosion and suppresses the formation of Li^0 dendrites.[26] Here, we work with two formulations, a 1 M LiFSI in pure DMC and a 1 M LiFSI in pure FEC. For these AIMD simulations, the packing procedure is applied as with the pure solvent formulations, but for the cell size, we increase the z-coordinate to 17.5 Å while leaving the other two coordinates unchanged at 12.5 Å. This cell size increment provides room to facilitate a solvation shell formation around the Li^+ ion while keeping the computational cost manageable. We found that the adsorption/decomposition mechanisms of the LiFSI salt are independent of the solvent of choice. Similarly, LiFSI does not affect the solvents' dynamics with the lithiated SPAN surface. Earlier works with lithium metal reported similar behavior.[16] Hence, calculations of LiFSI decomposition with other solvent species were not included in this work.

Figure 2 shows the solvation shells formed for both formulations throughout the simulations. From (a) to (c), for the 1 M LiFSI/DMC formulation, we find that the FSI^- anion not only interacts with the Li^+ ion via two or one sulfonyl oxygen atoms (bidentate and monodentate configurations) but also exists as a separated anion without direct interaction with the Li^+ ions. The FSI^-'s ability to adapt to these multiple configurations in the solvation shell comes from its low N-S bond rotation barrier,[43, 44] which reportedly inhibits salt crystallization within a broad concentration span.[45] Meanwhile, the DMC molecules complete the tetrahedrally coordinated

solvation shells, and most of them coordinate with the Li^+ ion via the carbonyl oxygen (O_1), with only one of them doing it via the ester oxygen atom (O_2). Moreover, Figure 2 (c) shows one DMC molecule settled in its trans-cis conformation with C_s symmetry.[42] We find this symmetry conformation only in simulations with the LiFSI salt and attribute this behavior to steric effects with the neighbor DMC molecules building up the solvation shell around the Li^+ ion.

Figure 2 (d) to (g) shows the solvation shells formed for the 1 M LiFSI/FEC formulation. The FSI^- anion engages in similar interactions with the Li^+ ion as with the formulation with the DMC solvent, whereas the FEC molecules complete the tetrahedral solvation shell coordinating with the Li^+ ion via the carbonyl oxygen (O_1) exclusively.

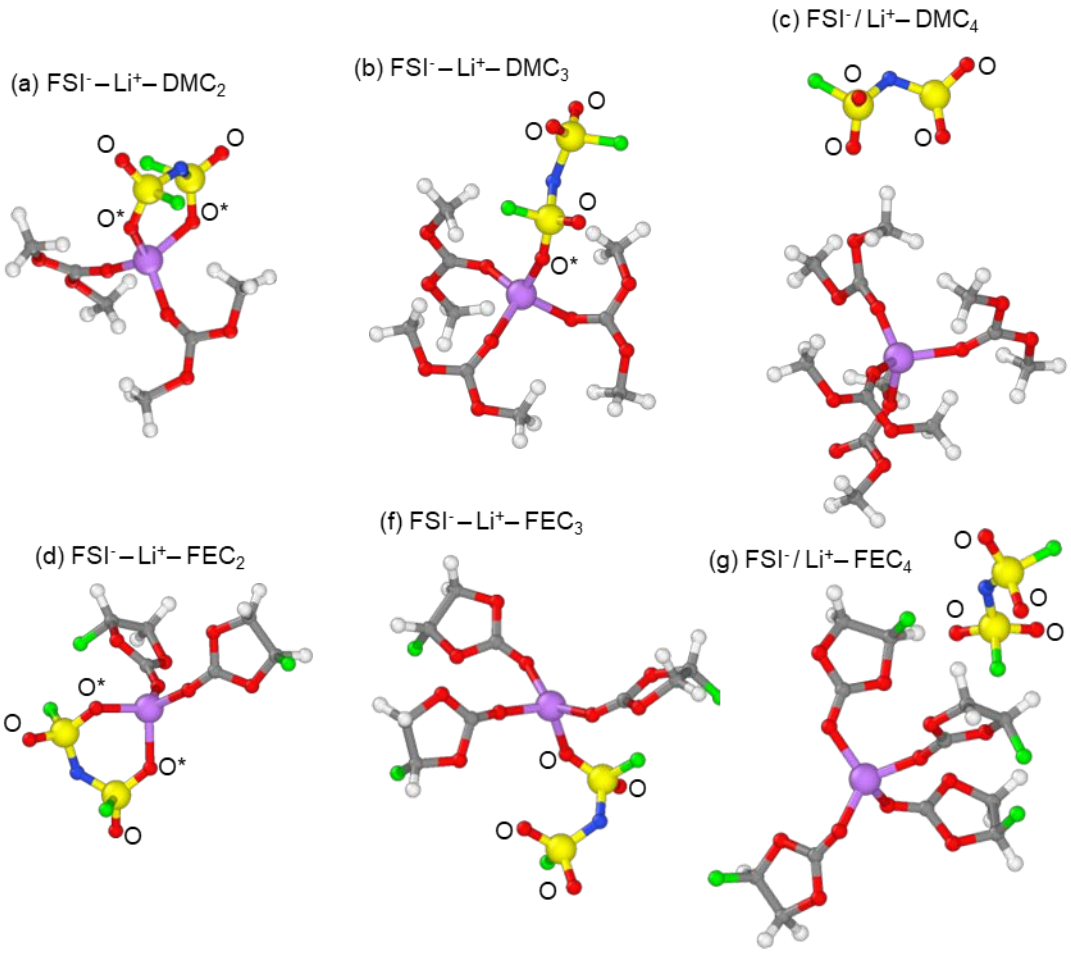

Figure 2: Solvation shells formed in 1M LiFSI/DMC: (a), (b), and (c). Solvation shells formed in 1M LiFSI/FEC: (d), (f), and (g). Background solvent molecules are not shown for easier visualization purposes. Sulfur atoms are the yellow spheres, nitrogen atoms are the blue spheres, and lithium is purple. Color spheres for carbon, oxygen, fluorine, and hydrogen are the same as in Figure 1.

Lithiated SPAN Surfaces

To model the interaction between the SPAN composite and the electrolyte, we use the SPAN structures built in our earlier publication on the lithiation mechanism, [46] where we reported the detailed procedure to assemble our models. This was a multistep procedure involving a high degree of randomness such that the resultant structures can be considered statistically representative of the SPAN structure. Thus, we estimate that our structures' surface landscapes do not have a strong influence on the simulation results beyond the impact that the lithium content induces. Note that here we are investigating interfacial reactions, therefore is the structure and chemistry of the exposed surface what matters most. These structures possess a carbon skeleton with a high graphitization degree, turbostratic ordering, and a 42 wt. % sulfur loading. Moreover, the C/N and C/H molar ratios are 4.21 and 7.37; very close to experimental data reported for SPAN composites synthesized from PAN and PAN/PMMA pyrolyzation processes.[6, 47-49]

We do not explicitly model the voltage discharge as we neither apply any electric bias nor let the number of electrons change to achieve the desired electron chemical potential at the electrode/electrolyte interface.[50, 51] However, our simulations still provide valuable insights into the electrode/electrolyte interface's reaction mechanisms as the increment in the lithium content in the electrode composite correlates to the discharge stage.[20] The SPAN composite produces a single and slightly sloped discharge voltage starting approximately at 2.0 V vs. Li/Li^+.[8, 9] In its charged state, the composite possesses no Li^+ ions. Once the discharge progresses, a 1.0 Li/S molar ratio is equivalent to a discharge voltage of 1.45 V vs. Li/Li^+.[46] Moreover, if the Li/S ratio equals 2.0, the discharge voltage is 1.0 V vs. Li/Li^+, and further increase to a 2.5 Li/S molar ratio represents a 0.55 V discharge voltage. Finally, the discharge ends at 0 V vs. Li/Li^+ when the Li/S molar ratio in the SPAN composite reaches a value of 3.0.

Figure 3 (a) shows a side view of the SPAN composite before lithiation, replicated along the x-coordinate. Periodic boundary conditions apply to each coordinate, but the graphitized skeleton orients along the y-z plane despite the defects and wrinkles present in the structure, allowing us to add a 15 Å gap along the x-coordinate to make room for the electrolyte molecules.[16] This slab-like arrangement maximizes the contact area between the composite and the electrolyte solution. The electrolyte molecules occupy the in-between vacuum space following the same packing procedure we employ for the liquid bulk calculations. Figure 3 (b), (c), (d), and (e) represent the lithiated SPAN composite with Li/S molar ratios equal to 1.0, 2.0, 2.5, and 3.0, respectively.

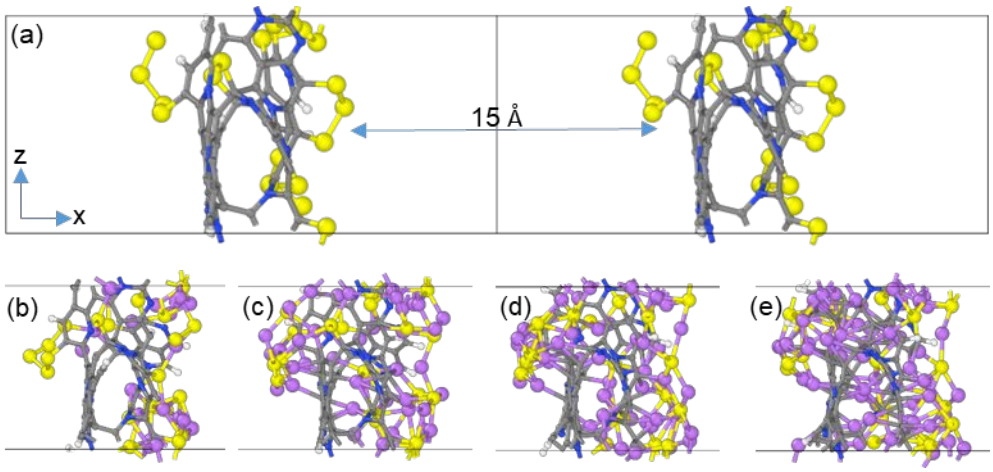

Figure 3: Side view SPAN models with varying Li/S molar ratios: (a) 0.0, (b) 1.0, (c) 2.0, (d) 2.5, and (e) 3.0. Color code for atoms as in Figure 2.

Electrolyte/SPAN Interface

Ether DOL Solvent

We packed between 14 to 18 DOL molecules in the in-between slab space as the Li/S molar ratio increases from 0.0 to 3.0 and created two initial configurations for each case to account for a broader statistical sampling. Figure S1 shows two simulation frames selected close to the end of the simulation, with the DOL molecules interacting with the SPAN composite before lithiation and with a 3.0 Li/S molar ratio. Notice from the figures that we slightly increased the vacuum space along the x-coordinate with the increase in lithium content to account for the volume expansion due to lithiation; in this way, the number of solvent molecules in the simulation remains almost constant regardless of the stage of discharge.

Figure 4 (a) shows a DOL molecule interacting with the surface interact via electrostatic O_2 – Li^+ ion interactions (see Figure 1 for atomic labels). The average distance for the O_2 – Li^+ interactions is 2.11 Å. None of the molecule's bond distances change more than 0.03 Å compared to the gas phase configuration, and the molecule's electronic charge does not change more than -0.04 |e| compared to that in the bulk liquid. Figure 4 (b) depicts the time evolution for the O_2 – Li^+ interactions for this molecule and shows us that these electrostatic interactions do not lead to a significant electron exchange with the surface. This is in agreement with the calculated reduction potential of 1.27 V [52] suggesting high stability for DOL complexes with Li^+.

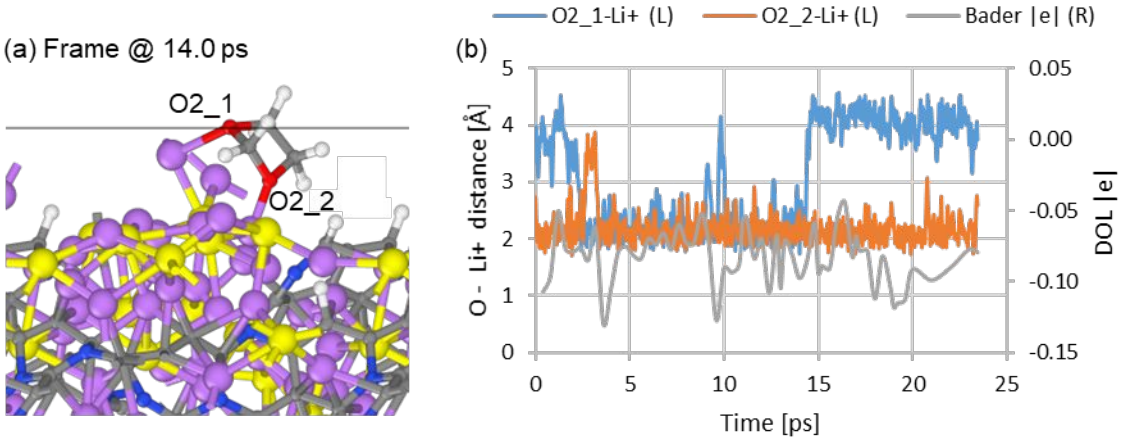

Figure 4: DOL adsorption on lithiated SPAN (Li/S molar ratio = 3.0): (a) Geometry configuration for a DOL molecule interacting with the lithiated SPAN surface at 14 ps of simulation, (b) O_2 – Li^+ ion coordination interactions and Bader electronic charge for the same DOL molecule throughout the simulation. Color code for atoms as in Figure 2.

Figure 5 shows the number of DOL molecules per unit area interacting with the SPAN surface via O_2 – Li^+ interactions. All simulations require at least six ps before stabilizing. Afterward, the increment in the Li/S molar ratio from 1.0 to 2.0 increases the number of molecules interacting with the surface from 0.020 to 0.039 DOL molecules per unit area ($Å^2$). However, any further increase in lithium loading does not induce significant changes, as the average number of molecules adsorbed per unit area averages at 0.042 and 0.039 for the surfaces with 2.5 and 3.0 Li/S molar ratios.

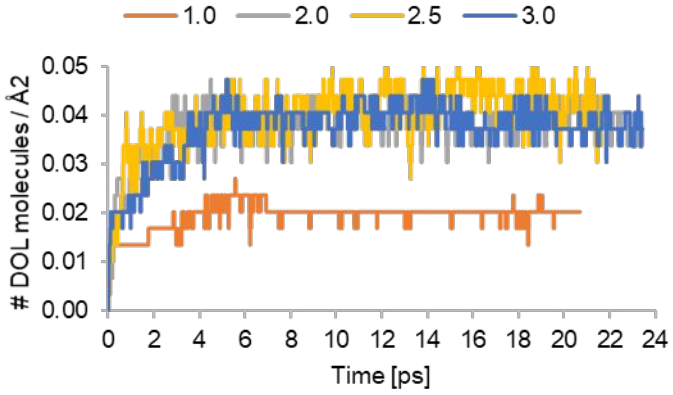

Figure 5: Number of DOL molecules per unit area adsorbed on the structure surface with increasing Li/S molar ratios.

Figure S2 plots the SPAN's net electronic charge throughout the simulation for each of the studied Li/S molar ratios. For a solvent reduction to occur, at least one electron must transfer into the molecule. However, neither simulation reaches a solvent/SPAN electron exchange

higher than 0.7 |e|; hence no DOL reduction occurs. A visual inspection of the DOL molecules at the end of the simulations confirms this affirmation. Neither the molecules that are interacting with the surface via O_2 – Li^+ interactions, nor the ones embedded in the liquid far from the surface show sign of a significant geometry deformation that could lead to a bond-breaking event.

Overall, the DOL interacts with the lithiated SPAN surface O_2 – Li^+ coordination, but this process does not lead to adsorption/decomposition processes; hence the DOL solvent most likely does not contribute to growing SEI coating on the SPAN composite. This affirmation agrees with scanning electron microscopy (SEM imaging performed on SPAN-based Li-S batteries cycled with ether-based electrolyte formulations with DOL; the cathode's surface does not show evidence of an SEI layer on the cathode surface after repeated cycling.[11] Electrochemical testing of a SPAN-based Li-S battery with a 1 M LiTFSI DOL/1,2-dimethoxyethane (DME) electrolyte provides further prove into this subject.[8] The battery shows not only rapid capacity fading but also a two-step discharge profile after the second cycle, meaning the electrode starts following a solid-liquid-solid reduction mechanism forming long-chain LiPSs that potentially diffuse into the bulk electrolyte,[53] likely linked to the ether solvent's inability to grow an SEI coating protecting the cathode.

Pure Carbonic Ester Solvents

Linear carbonate DMC

DMC is a linear symmetric carbonate of general use as co-solvent with fluorinated carbonates,[17, 21] acting as a viscosity reducer that produces Li-S batteries with excellent rate performance and long lifespan.[54] Figure 6 (a) plots the net electron exchange between the DMC solvent and the lithiated SPAN composite with a 3.0 Li/S molar ratio. For the two initial configurations we created (v1 and v2), the electron exchange remains lower than 0.75 |e| throughout the simulation, with no noticeable step increments that might hint at a solvent reduction process about to take place. The average electron transfer to each DMC molecule is -0.04 |e| with a slightly higher transfer to those DMC molecules closer to the surface. We did not evaluate the interfacial DMC/SPAN interaction with DMC molecules for SPAN composites with lower Li/S molar ratios because the solvent is already stable with a 3.0 Li/S molar ratio, and the electrolyte reduction reportedly occurs in later stages of discharge only.[14]

The interaction between the DMC molecules and the lithiated surface is via O_1 – Li^+ ion coordination. A visual inspection of Figure S3 shows that the O_1 – Li^+ interaction dominates, with

only a few DMC molecules interacting with the surface via O_2 – Li^+ coordination. Figure 6 (b) depicts the number of DMC molecules per unit area interacting with a lithiated SPAN surface with a 3.0 Li/S molar ratio. As with the simulation with the DOL solvent, the simulation stabilizes within the first six ps. After that, the simulation averages at 0.028 DMC molecules per unit area interacting with the lithiated surface. We plotted the results for the v2 configuration only, but the v1 configuration has a low average of 0.034 DMC molecules per unit area ($Å^2$). A visual inspection of the geometry by the end of the simulation shows that DMC molecules' areal density interacting with the surface does not increase further due to steric effects between surrounding DMC molecules. This simulation set shows that the DMC solvent does not reduce against the lithiated SPAN surface even though the 3.0 Li/S molar ratio; hence the DMC solvent does not play a significant role in growing a passivation SEI coating on the SPAN composite but merely act as a viscosity reducer when used along with other cyclic carbonate solvents.[54]

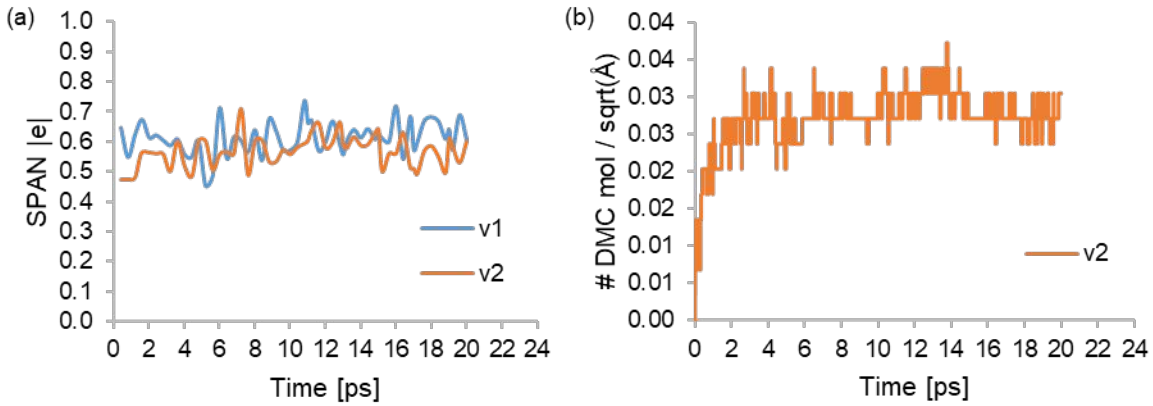

Figure 6: (a) Time evolution of the SPAN surface electronic charge at 3.0 Li/S molar ratio: first (v1) and second (v2) configurations. (b) Number of DMC molecules per unit area ($Å^2$) adsorbed on lithiated SPAN (3.0 Li/S molar ratio): second configuration (v2).

Cyclic carbonate EC

The discharge voltage window of SPAN-based Li-S battery systems typically spans between 3 - 1 V vs. Li/Li^+, where most electrolytes are electrochemically stable.[14] Hence, to promote the SEI growth on SPAN composites, one must either induce a high potential to promote electrolyte oxidation reactions or perform the battery discharge following an over-discharge regime to voltages lower than 1 V vs. Li/Li^+.[14] Experiments show that SPAN-based Li/S batteries have improved performance and extended capacity retention only if over-discharged to 0 V vs.

Li/Li^+.[13, 55] Conversely, the battery does not produce any extra reversible capacity but fails if over-charged above 3.8 V vs. Li/Li^+.

Figure S4 (a) and (b) show the partial radial distribution function (PRFD) profiles averaged for the last two ps for the S-O, S-F, C-O, and C-F interactions for the EC molecules with the SPAN composite before lithiation. Notice that each AIMD simulation (configurations v1 and v2) runs for no less than 23 ps. The analysis of these interactions helps us discard possible adsorption mechanisms before discharge that could lead to spontaneous solvent oxidation at a high voltage. Compared to DMC, EC has been reported as a coating-forming solvent more active to grow SEI coatings.[11, 16, 56] From the PRDF profiles; we observe no solvent interaction with the surface. The EC's carbonyl oxygen atom (O_1) does not coordinate with neither sulfur nor carbon atoms from the SPAN composite. The time evolution for the composite/solvent electron exchange in Figure S5 confirms our observation; the total electron exchange is less than 0.35 |e| in all simulations, meaning no solvent decomposition on the surface. The SEI growth via EC decomposition does not likely happen before the discharge starts.

We also study the interfacial interaction between EC and lithiated SPAN with Li/S molar ratios equivalent to discharge voltages from 1.0 to 0.0 V vs. Li/Li^+. Figure S6 shows the time evolution for the EC/SPAN electron exchange for SPAN surfaces with Li/S molar ratios: 2.0, 2.5, and 3.0. The electron exchange becomes significant only for the SPAN surfaces with a 3.0 Li/S molar ratio. This behavior suggests that the EC reduction most likely happens in an over-discharge regime close to the end of the discharge, which might explain why the SEI coatings grown on cathode surfaces are typically extremely thin;[57] because typical battery operating potentials rarely reach voltages low enough for the electrolyte reduction reactions on the SPAN surface to become significant.

Figure 7 shows two EC molecules dissociated on the lithiated SPAN surface (3.0 Li/S molar ratio) following a dissociation mechanism similar to the one reported for EC on graphitic anodes, lithium metal surfaces, and lithiated silicon anodes.[20] The molecule's adsorption starts with O_1-Li^+ ion interactions followed by O_2 – Li^+ interactions. The molecule receives a two |el transfer from the surface that triggers the C_1-O_2 bond cleavage that leads to the formation of the $O(C_2H_4)OCO^{2-}$ species that remains adsorbed on the surface via multiple O – Li^+ ion coordination interactions. Earlier works point at the C_1-O_2 bond as the weakest in EC-Li^+ complexes.[58] The C_1-O_2 bond reportedly breaks irreversibly upon adsorption on lithium metal anodes.[16, 59]

$EC_{(ads)} + 2e^- \rightarrow O(C_2H_4)OCO^{2-}{}_{(ads)}$ Eq. 1

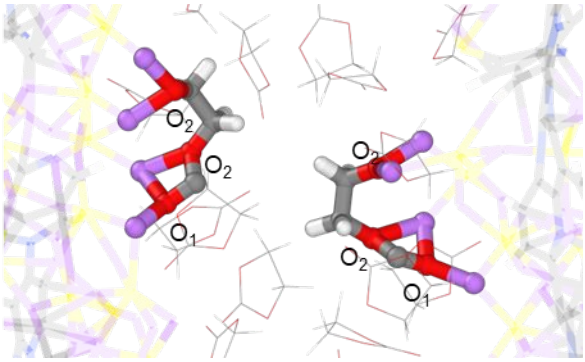

Figure 7: EC ring-opening decomposition on lithiated SPAN (3.0 Li/S molar ratio). The snapshot highlights reduction products and the Li^+ ions engaged in O – Li^+ ion coordination interactions. The SPAN surface is displayed as semitransparent, and the other EC molecules are shown in thin line representations for better visualization. Color code for atoms as in Figure 2.

Figure 8 shows the decomposition path for other three EC molecules on the lithiated SPAN surface (3.0 Li/S molar ratio). The molecules labeled as 4.ec and 11.ec adsorb on the SPAN surface via O_1 – Li^+ coordination. For the molecule 4.ec, Figure S7 shows that the O_1 – Li^+ distance oscillates around 1.94 Å. After approximately nine ps, the molecule reorients in space to further engage in O_2 – Li^+ ion interactions at 1.78 and 1.83 Å approximately. This adsorption mechanism triggers a simultaneous two |e| transfer into the molecule that prompts the sequential cleavage of both C_1-O_2 bonds within a two ps period. The reduction products are an $OCH_2CH_2O^{2-}$ species that remains adsorbed via multiple O – Li^+ ion coordination interactions and a CO species that diffuses away into the bulk liquid. Eq. 2 summarizes this process:

$EC + 2e^- \rightarrow OCH_2CH_2O^{2-}{}_{(ads)} + CO_{(Liq)}$ Eq. 2

Eight ps later, the CO becomes a radical after close interactions with an H atom from a surrounding EC molecule. The CO molecule breaks, and the C radical destabilizes the neighbor molecule (10.ec), promoting its decomposition in the liquid phase. The decomposition starts with an H abstraction and concludes with an HCCH molecule, an OCH_2^{1-} radical, and a CO_2 molecule. The HCCH molecule remains in the liquid phase, and the OCH_2^{1-} radical adsorbs on the surface via O – Li^+ ion coordination. The CO_2 molecule bonds form a C-C bond with the OCH_2^{1-} radical forming the $O_2CCOH_2^{2-}{}_{(ads)}$ species that remains adsorbed via O - Li^+ interactions. We interpret the formation of these complex reduction products as the onset stages of a series of radical polymerization and cross-linking of polymer chains that could yield a robust and elastic coating able to withstand volume changes during lithiation/delithiation processes.

Parallel to this process, the O^- radical released after the C-O scission removes one H atom from the 11.ec molecule. This OH^- species coordinates with two Li^+ ions, and the rest of the 11.ec molecule suffers an O_2-C_3 cleavage. The $O_2COCHCH_2^-{}_{(ads)}$ species remains adsorbed on the surface via multiple O – Li^+ ion coordination interactions.

This reaction series set shows that the EC solvent is very active in the growth of an SEI coating on SPAN composites if the discharge regime goes to low voltages close to 0.0 V vs. Li/Li^+, which means that the SEI coating mostly forms when the SPAN volume is maximum due to the high lithium content, potentially bringing long-term mechanical stability.[21]

The CO species released in Eq. 2 triggers a cascade of reactions in other EC molecules, either in the liquid phase or adsorbed, leading to the early growth stages of a complex organic-based passivation coating on the SPAN surface. Notice that this process also leads to a series of S – Li^+ bond-breaking events; hence the SEI growth from EC reduction products also implies a surface reconstruction process, which could imply irreversible loss of some Li^+ ions. Because the SEI coating forms during the first cycle mostly, we believe this could explain the irreversible capacity loss between the first and second cycles.[8] The pDOS analysis in Figure S8 performed for selected frames helped out to identify the radical species involved in this sequence of decomposition reactions. The highly reactive EC behavior is in agreement with previous analysis of SEI formation on carbon and silicon surfaces. Interestingly, DMC and EC behave differently on the lithiated SPAN surface in spite of their reported similar reduction potentials,[60] showing the important role of the surface/electrolyte interaction.

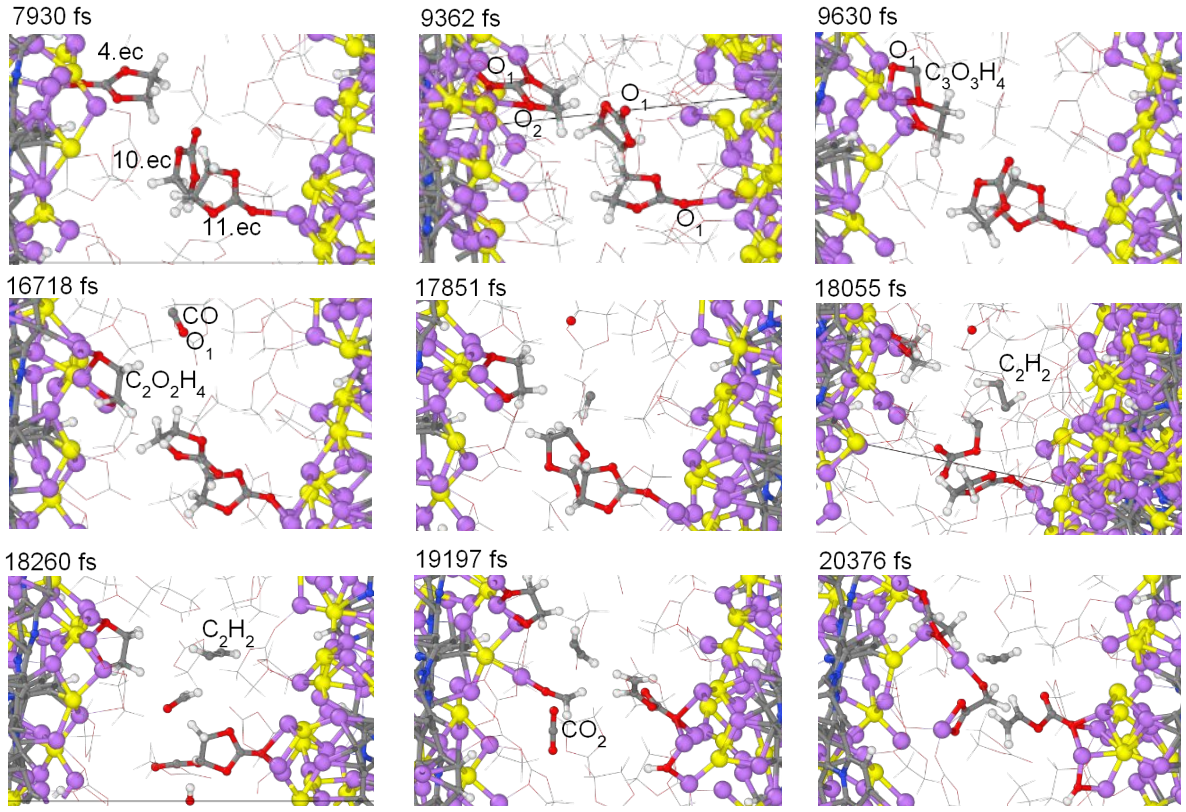

Figure 8: Events during EC reductive decomposition at the surface and in the liquid phase. Color code for atoms as in Figure 2.

Cyclic Carbonate FEC

The FEC solvent is an additive frequently used in EC-based formulations because it easily defluorinates in reduction reactions.[18] This defluorination process facilitates radical polymerization and cross-linking of polymer chains yielding an elastic coating capable of withstanding the stresses cause due to volume changes during lithiation/delithiation processes as it occurs in Li_xSi_y electrodes. Higher cross-linking correlates with denser and thinner SEI coatings, as reported for SEI coatings grown on silicon anodes.[61] This property potentially contributes to better SEI coatings on sulfur-based electrodes as the lithiation of elemental sulfur leads to an 82 % volume expansion.[62]

Figure S9 plots the electron exchange between the FEC solvent and the lithiated SPAN composite with Li/S molar ratios equal to 2.0 and above. The electron exchange becomes significant from a 2.0 Li/S molar ratio. For the EC solvent, Figure S6 shows that the electron exchange is relevant only after the SPAN composite reaches a 3.0 Li/S molar ratio. Compared to EC, earlier FEC decomposition is reported on silicon anodes,[21] which makes the FEC a

useful additive in EC-based formulations as it might help prevent uncontrolled EC decomposition. Moreover, MP2 calculations predict the FEC:Li^+ reduction potential to be 0.22 V higher than EC:Li^+, suggesting that the FEC accepts an electron at higher voltages than EC.[20]

Figure 9 (a) outlines the decomposition steps for an FEC molecule on lithiated SPAN with a 2.0 Li/S molar ratio. Like the EC molecule, the FEC molecule approaches the surface via O_1 – Li^+ coordination followed by O_2 – Li^+ interactions. However, this time carbonyl carbon (C_1) coordinates with a sulfur atom triggering a two |e| transfer into the molecule that promotes the C_1-O_2 bond cleavage. The adsorbed $OCFHCH_2O^{2-}$ species experiences a fluorine abstraction reaction to form a LiF on the surface. Figure 9 (b) shows the same reduction products for an FEC molecule reduced on a lithiated SPAN composite with a 2.5 Li/S molar ratio. Eq. 3 summarizes this reduction process that proceeds within a few ps period.

$$FEC_{(ads)} + 2e^- + Li^+ \rightarrow OCFHCH_2O^{2-}{}_{(ads)} + Li^+ \rightarrow OCHCH_2O^-{}_{(ads)} + LiF \qquad \text{Eq. 3}$$

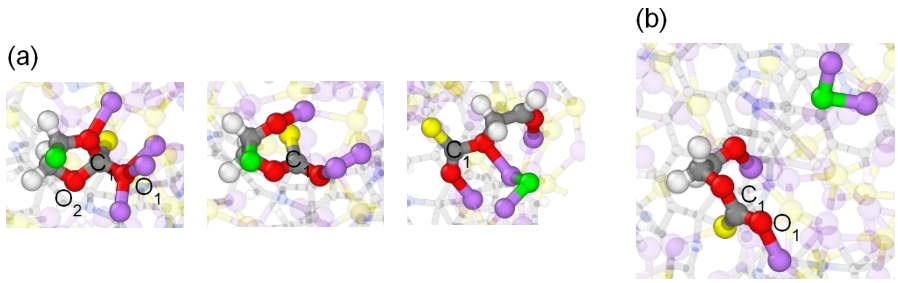

Figure 9: (a) FEC decomposition on lithiated SPAN with a (a) 2.0 Li/S molar ratio and (b) 2.5 Li/S molar ratio. Atomic coloring as in Figure 2.

Figure 10 shows the reduction species for three FEC neighbor molecules on a lithiated SPAN composite with a 3.0 Li/S molar ratio. The 2.fec molecule follows the same reduction mechanism outlined in Eq. 3 except for the F abstraction reaction. We believe the reduced $OCFHCH_2O^{2-}{}_{(ads)}$ species eventually undergoes the fluorine abstraction process, but the specific species orientation limits the Li-F interaction, and the time simulation window was too short for it to occur. On the other side, the 12.fec molecule approaches the surface via F – Li^+ ion coordination that triggers a one |e| transfer into the molecule. The C-F bond breaks forming LiF and $OCFHCH_2O^{2-}$. This reactive $OCFHCH_2O^{2-}$ species interacts with a neighbor FEC molecule (10.fec) to form a C_2-C_1 bond. This bonding interaction transfers one |e| into the neighbor FEC molecule (10.fec); hence the total electron transfer equals two |e|. We believe a further defluorination could occur for this complex structure, but the simulation time window was too short to allow observation. We note that FEC defluorination effectively leads to oligomerization

and cross-linking processes that contribute to elastic SEI coatings, as reported for Li_xSi_y electrodes.[18] This reduction mechanism resembles the one proposed by Etacheri et al.;[63] the defluorination produces LiF and ends up polymerizing into poly(VC).[64]

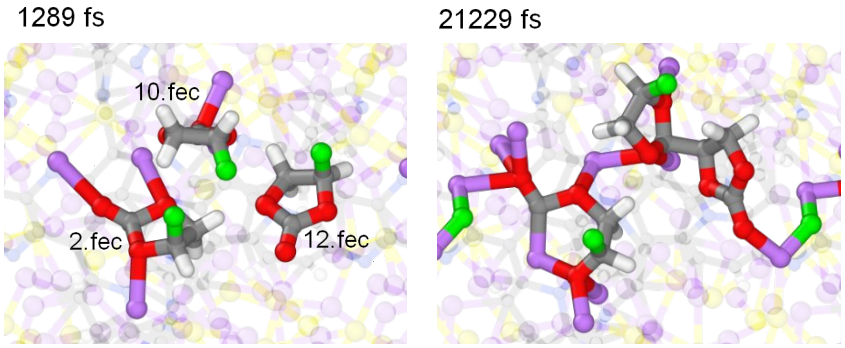

Figure 10: FEC decomposition and oligomerization processes on a lithiated SPAN surface with a 3.0 Li/S molar ratio. Color code for atoms as in Figure 2.

Figure 11 outlines other decomposition paths for FEC molecules on the lithiated SPAN surface with a 3.0 Li/S molar ratio. The 1.fec molecule interacts with the surface via O_1 – Li^+ interactions and a double C_1-O_2 scission take place after receiving one |e| from the surface.

The CO species remains on the surface via O – Li^+ and C – Li^+ interactions, but it eventually breaks into O and C. The O coordinates with four Li^+ ions, and the C diffuses away into the liquid phase. The OCH_2CFO^{2-} remains on the surface via O – Li^+ interactions, but it eventually losses the F^- anion to the liquid phase, and the OCH_2CO^- remains on the surface. The F^- anion does not get involved in further reactions within the simulation time window, but it is expected that it eventually adsorbs on the surface to form LiF.

The released C atom destabilizes the 2.fec molecule, and a series of bond-breaking events follow involving another neighbor FEC molecule (9.fec). This process ends up forming an $O_2COCH_2C_2F^-_{(ads)}$ species adsorbed on the surface via multiple O – Li^+ interactions exclusively, a cyclic $CHCHCO_{3(ads)}$ species, LiF, and H_2. The formation of multiple reduction products shows that the FEC solvent is very active in SEI coatings' growth on SPAN composites. The FEC's defluorination occurs on the surface and the liquid phase, and it not only promotes LiF formation but also triggers radical recombination/oligomerization, which is key to yielding elastic properties to the SEI coating.

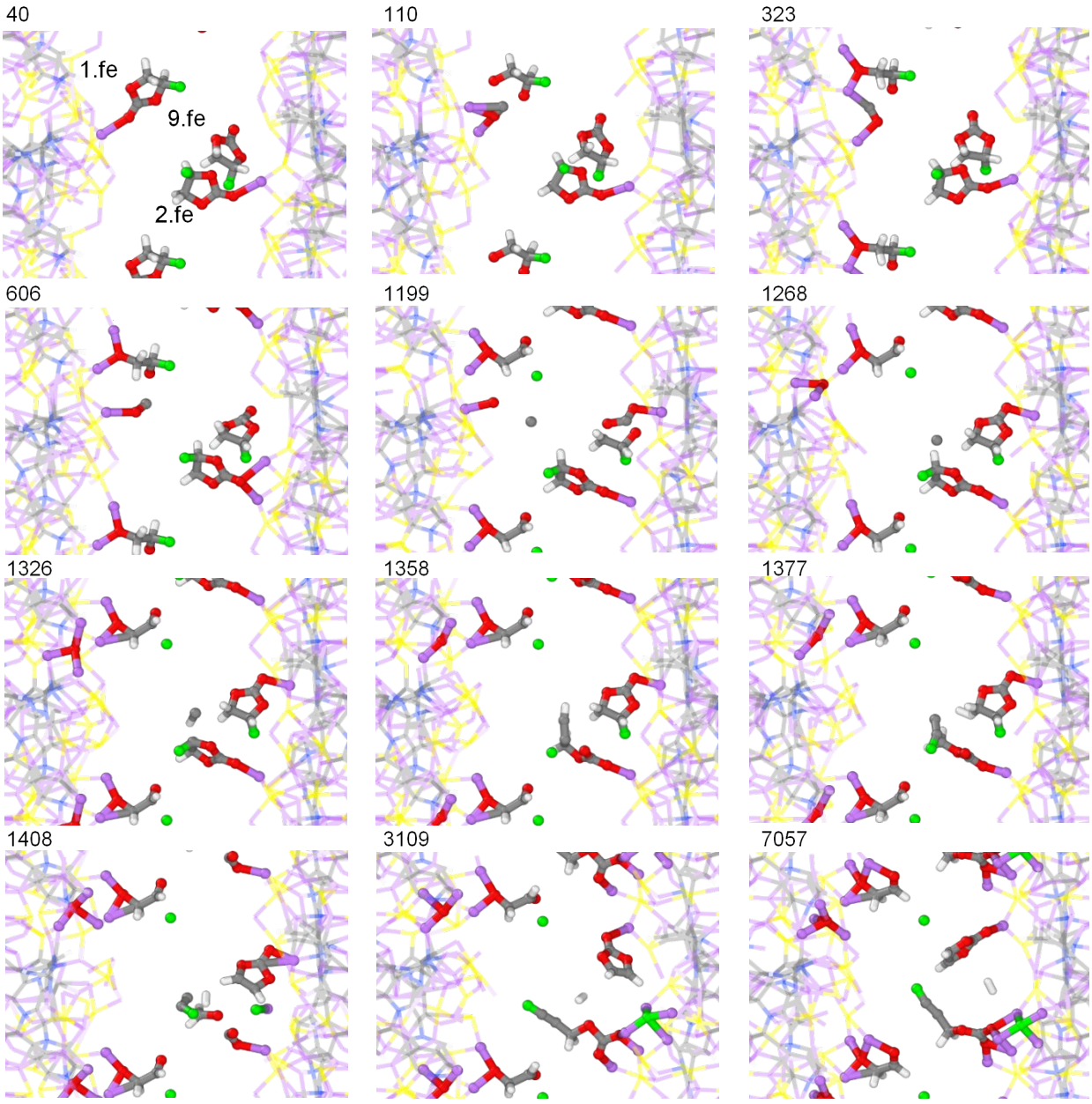

Figure 11: FEC reductive decomposition in the liquid phase. Color code for atoms as in Figure 2. See text for detailed description of events.

Salt/Solvent Mixtures

Fluorinated anions in ionic liquid electrolytes improve the performance of Li-ion batteries. For example, the $LiPF_6$ salt decomposes on silicon anodes to form a homogeneous LiF distribution, which is reportedly fundamental to growing a stable SEI,[65] not only on silicon anodes but also on metal anodes for Li-ion and Li-O_2 batteries.[21] A thin LiF layer stops electron tunneling and provides plasticity by dislocation glide, a rare property among ceramics at room temperature.[25,

[66] On the other side, the LiFSI salt has surfaced as a viable alternative to the typical LiTFSI because it produces electrolyte formulations with low viscosity and high chemical stability, inhibits electrolytic corrosion, and can grow robust SEI interfaces to protect the electrolyte against further decomposition.[26]

We address the LiFSI decomposition on lithiated SPAN with a 3.0 Li/S molar ratio. To do so, we fill the vacuum space in our model with a 1 M LIFSI electrolyte solution in pure DMC and pure FEC solvents. The limited space available in the simulation cell is such that we only add one LiFSI molecule to it and fill the remnant space with the solvent molecules, following the same packing procedure used before for pure solvents. We test two configurations for each solvent, first with the FSI^- anion in an initial bidentate configuration with the Li^+ ion, and second with a separated FSI^- anion, with the Li^+ ion fully solvated with solvent molecules.

LiFSI/DMC

Figure 12 shows the time evolution for the FSI^- anion in an initial bidentate configuration with the Li^+ ion. This Li^+ ion is present in addition to the Li^+ ions from the lithiated SPAN composite. We acknowledge that this Li^+ ion is subject to a desolvation process to become part of the lithiated surface. However, we do not expect this to happen because of the already high Li/S ratio in the lithiated structure and the limited time simulation window. Besides, the simulation does lack an external bias driving the desolvation process.[67] The initial distance from the closest lithiated SPAN surface to the FSI^- anion is close to five Å. Even though this considerable distance, the FSI^- anion suffers a fluoride elimination within the first two ps of simulation, the F atom goes to the surface to bond to a Li^+ ion forming a LiF pair, and the $SO_2NSO_2F^-$ radical remains in the liquid phase close to the surface engaged in a bidentate configuration with the solvated Li^+ ion. The Bader charge analysis shows that the defluorination process involves a one |e| transfer into the FSI^-. No DMC molecules decompose in the simulations. We believe that this reductive defluorination process is due to an electron tunneling current between the surface and the solvated FSI^- anion, which has been proposed too for liquid-phase reduction processes of carbonate solvent molecules.[56, 68] Earlier computational and experimental works proposed this same defluorination mechanism for the FSI^- anion in the liquid phase and on a Li(001) surface.[26] The LiF pair behaves stable within the simulation window; we observe transient Li_2F and Li_3F structures at some stages of the simulation, in agreement with earlier simulations of LiFSI-based ionic liquids on metal lithium anodes,[69] and reactive classical molecular dynamics simulations.[70] The $SO_2NSO_2F^-$ radical does not undergo further decomposition reactions. Other works link the stability of the $SO_2NSO_2F^-$ radical to yield a inorganic SEI layer without SO_2

elimination. This importance of arresting the SO_2 release relies on limiting gaseous products that could compromise the SEI integrity.[26]

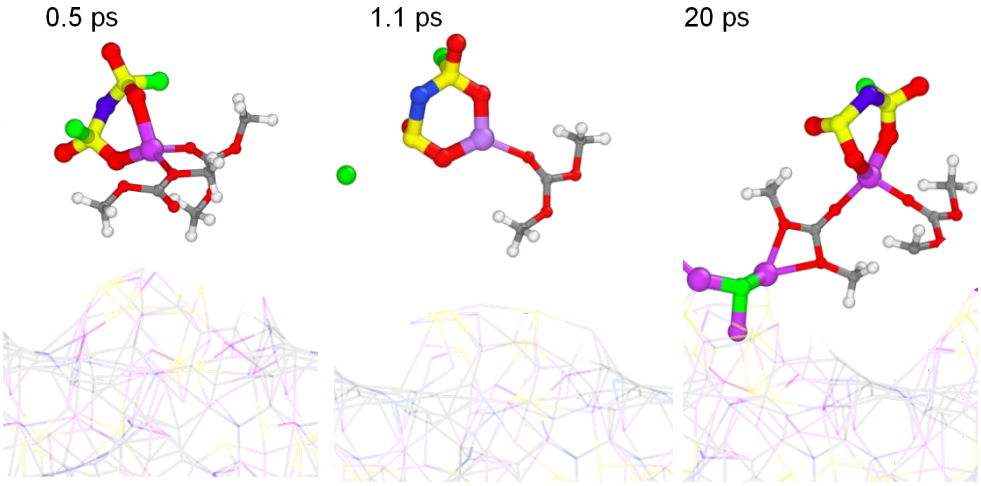

Figure 12: 1 M LiFSI in DMC with a lithiated SPAN surface (3.0 Li/S molar ratio). The FSI^- anion defluorinates in the liquid phase. Color code for atoms as in Figure 2.

Figure 13 shows the decomposition path for the FSI^- anion separated from the solvated Li^+ ion initially. The FSI^- engages with the solvated Li^+ within the first ps of simulation, and it loses a fluorine atom to the lithiated surface within the next ps to form LiF. The $SO_2NSO_2F^-$ radical does not undergo further defluorination, but it adsorbs on the surface via multiple O – Li^+ ion coordination interactions. We attribute the ability of the $SO_2NSO_2F^-$ radical of engaging multiple – Li^+ interactions to the low rotation barrier of the S-N bonds, calculated to be only 0.18 eV via DFT calculations.[26]

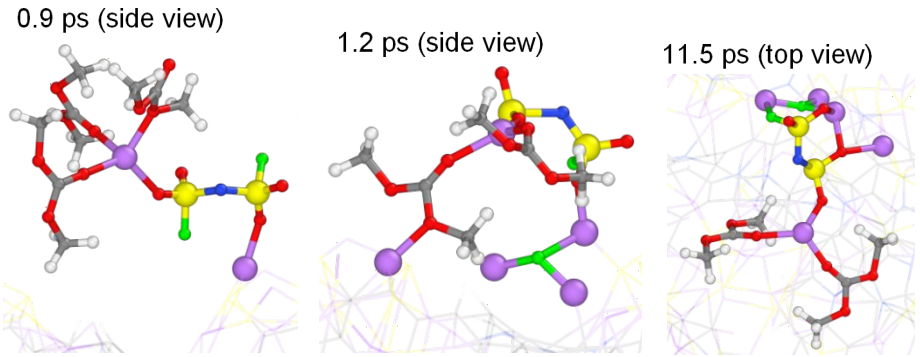

Figure 13: 1 M LiFSI in DMC with a lithiated SPAN surface (3.0 Li/S molar ratio). The defluorinated FSI- anion adsorbs on the surface via multiple O – Li^+ ion coordination interactions. Color code for atoms as in Figure 2.

LiFSI/FEC

The first configuration corresponds to the FSI^- ion in an initially bidentate arrangement with the Li^+ ion away from the surface. Figure 14 shows a selected frame close to the end of the simulation highlighting the FSI^- ion in the liquid phase and two FEC molecules that undergo a reduction process on the surface. The FSI^- separates from the solvated Li^+ ion and does not suffer any defluorination. The average distance from the surface is close to 6.2 Å, which seems large enough to hinder an electron tunneling-driven defluorination as it occurred with the DMC solvent. Conversely, two FEC molecules undergo a reductive decomposition on the lithiated SPAN surface. The first one is an FEC molecule initially solvating the Li^+ ion. This molecule receives a four |e| transfer that triggers its defluorination and the simultaneous C_2-O_2 cleavage to produce $CO_2^{2-}{}_{(ads)}$, a CH_2CHO^- species, and a F^- atom that ends up bonding to a Li^+ ion to form LiF. This four |e| reduction mechanism seems promoted by the solvated Li^+ ion. Earlier calculations with1.2 M LiFSI formulations in DMC showed that solvent – Li^+ ion coordination lowers the molecule's LUMO level, increasing the molecule's likelihood to be reduced the surface.[71] The other FEC molecule suffers a simultaneous two |e| reduction mechanism as in Eq. 3 that triggers its defluorination and a C_2-O_2 bond cleavage to produce an $OCHCH_2O^{2-}{}_{(ads)}$ species and LiF.

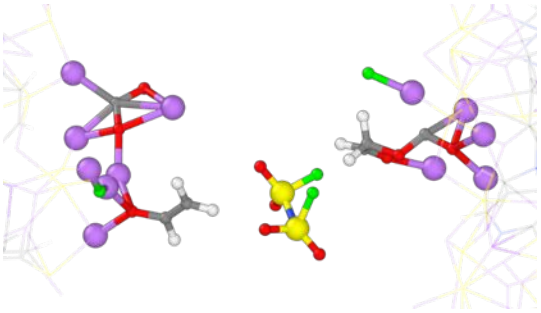

Figure 14: 1M LiFSI in FEC with a lithiated SPAN surface (3.0 Li/S molar ratio). The FSI- anion locates away from the surfaces and does not defluorinate. Color code for atoms as in Figure 2.

Figure 15 shows a selected frame close to the end of the simulation for the second configuration. For this configuration, the FSI^- does not solvate any Li^+ and is initially located close to the surface. The FSI anion suffers a simultaneous two |e| transfer, and it loses both F atoms to the surface. This reduction process produces LiF and a $SO_2NSO_2^{2-}{}_{(ads)}$ that remains on the surface via multiple O – Li^+ ion coordination interactions. Eq. 4 summarizes this reduction mechanism. The low rotation barrier for the S – N bonds results fundamental to let the $SO_2NSO_2^{2-}$ orient the sulfonyl oxygen atoms towards the surface to engage in O – Li^+ ion

coordination interactions. This simulation also shows the stability of the S – N bonds to resist cleavage after defluorination, hindering the release of SO_2 into the liquid phase.

$LiFSI + 2e^- \rightarrow 2LiF + SO_2NSO_2^{2-}{}_{(ads)}$ Eq. 4

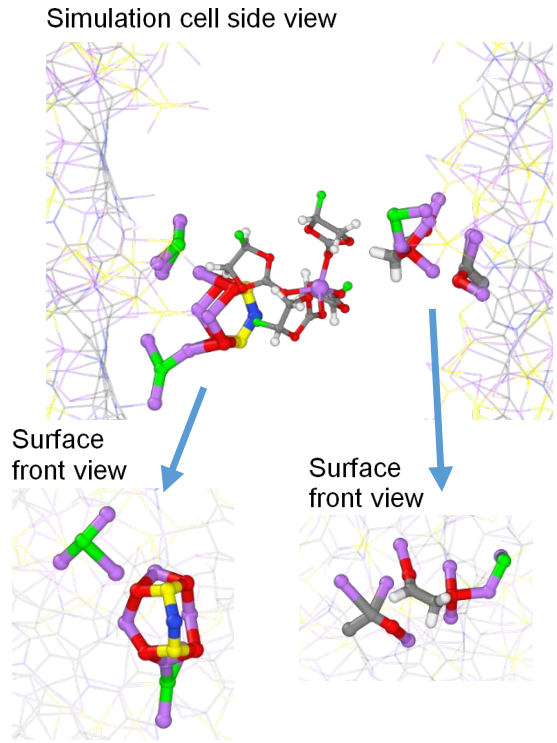

Figure 15: 1M LiFSI in FEC with a lithiated SPAN surface (3.0 Li/S molar ratio). The FSI- anion close to the surface suffers a double defluorination process. Color code for atoms as in Figure 2.

Conclusions

This work contributes to elucidating the important problem of the SEI formation on the cathode, which is crucial for battery long term stability. We evaluate the interfacial reactivity of multiple solvent species and a LiFSI salt on SPAN surfaces in multiple stages of lithiation via AIMD simulations. The ether DOL solvent is stable in contact with the SPAN surface regardless of the lithium content, proving that this solvent does not likely contribute to growing an SEI coating to protect the SPAN composite against polysulfide dissolution in normal battery operation conditions. The linear carbonate DMC interacts with the lithiated SPAN surface via O_1 – Li^+ ion coordination interactions but does not reduce. This solvent species' significant contribution to the battery performance is most likely acting as a viscosity reducer but not reducing the SPAN composite. The cyclic carbonate solvents EC and FEC prove to be very active as coating-forming species to strengthen the SPAN composite stability during cycling. The EC reduction

occurs only on the lithiated SPAN surface with a 3.0 Li/S molar ratio. This behavior suggests that SEI formation from EC most likely occurs if the battery, following an over-discharge regime close to 0 V vs. Li/Li^+ during the first cycle. The SEI growth on SPAN composites proceeds mostly during the first cycle. We observed the FEC reduction on lithiated SPAN surfaces from a 2.0 Li/S molar ratio and above, suggesting that FEC reduction starts at higher voltages than EC. This behavior makes the FEC an attractive additive to use alongside EC as it might help prevent uncontrolled EC decomposition. The FEC defluorination proves to be a dominant reduction step for this solvent that contributes to LiF formation.

Besides, the FEC undergoes multiple decomposition pathways that lead to oligomerization and cross-linking reactions. An SEI coating with a LiF phase and high cross-linking is potentially more stable against SPAN volume expansion behavior after discharge. The defluorination of the FSI^- anion is the predominant reductive path. However, the $SO_2NSO_2F^-$ and $SO_2NSO_2^{2-}$ species proved stable against S-N cleavage. This behavior makes the LiFSI salt a potential candidate for SPAN-based Li-S batteries because it produces LiF without releasing SO_2. We observed that FSI^- does not likely induce solvent decomposition, but the solvent molecules proved more likely to be reduced due to their coordination with the solvated Li^+ ion. These findings contribute to a better understanding of the reactivity of multiple solvent species and LiFSI on lithiated SPAN surfaces and provide a mechanistic view of the possible decomposition pathways followed in the SEI's early formation stages.

Supporting Information

Supporting information available includes: DOL/SPAN interfacial AIMD simulations (Fig. S1); Time evolution of the SPAN surface electronic charge with increasing Li/S molar ratios (Fig. S2); DMC interaction with the lithiated SPAN surface with a 3.0 Li/S molar ratio (Fig. S3); partial radial distribution functions for SPAN/EC interactions (Fig. S4); Time evolution of the SPAN electronic charge before lithiation for systems with EC and FEC (Fig. S5); Surface charge time evolution for EC with increasing lithium loadings (Fig. S6); O-Li^+ distance evolution for EC molecule (Fig. S7); projected DOS analysis for system in Fig. 8 (Fig. S8); Surface charge time evolution for FEC with increasing lithium loadings (Fig. S9). The POSCAR files for the SPAN computational model are available from the authors upon request.

Conflicts of Interest

There are no conflicts of interest to declare.

Acknowledgments

This material is based upon work supported by the U.S. Department of Energy's Office of Energy Efficiency and Renewable Energy (EERE), as part of the Battery 500 Consortium, Award Number DE-EE0008210. Supercomputer resources from the Texas A&M University High Performance Computer Center and Texas Advanced Computing Center (TACC) are gratefully acknowledged.

References

1. Barghamadi, M.; Kapoor, A.; Wen, C., A Review on Li-S Batteries as a High Efficiency Rechargeable Lithium Battery. *J. Electrochem. Soc.* **2013,** *160* (8), A1256-A1263.
2. Cano, Z. P.; Banham, D.; Ye, S.; Hintennach, A.; Lu, J.; Fowler, M.; Chen, Z., Batteries and Fuel Cells for Emerging Electric Vehicle Markets. *Nat. Energy* **2018,** *3* (4), 279-289.
3. Pang, Q.; Liang, X.; Kwok, C. Y.; Nazar, L. F., Advances in Lithium–Sulfur Batteries Based on Multifunctional Cathodes and Electrolytes. *Nat. Energy* **2016,** *1*, 16132.
4. Kim, H.; Wu, F.; Lee, J. T.; Nitta, N.; Lin, H.-T.; Oschatz, M.; Cho, W. I.; Kaskel, S.; Borodin, O.; Yushin, G., In Situ Formation of Protective Coatings on Sulfur Cathodes in Lithium Batteries with LiFSI-Based Organic Electrolytes. *Adv. Energy Mater.* **2015,** *5* (6), 1401792.
5. Wang, J.; Yang, J.; Xie, J.; Xu, N., A Novel Conductive Polymer–Sulfur Composite Cathode Material for Rechargeable Lithium Batteries. *Adv. Mater.* **2002,** *14* (13-14), 963-965.
6. Fanous, J.; Wegner, M.; Grimminger, J.; Andresen, Ä.; Buchmeiser, M. R., Structure-Related Electrochemistry of Sulfur-Poly(acrylonitrile) Composite Cathode Materials for Rechargeable Lithium Batteries. *Chem. Mater.* **2011,** *23* (22), 5024-5028.
7. Fanous, J.; Wegner, M.; Grimminger, J.; Rolff, M.; Spera, M. B. M.; Tenzer, M.; Buchmeiser, M. R., Correlation of the Electrochemistry of Poly(acrylonitrile)–Sulfur Composite Cathodes with their Molecular Structure. *J. Mater. Chem.* **2012,** *22* (43), 23240-23245.
8. Wei, S.; Ma, L.; Hendrickson, K. E.; Tu, Z.; Archer, L. A., Metal–Sulfur Battery Cathodes Based on PAN–Sulfur Composites. *J. Am. Chem. Soc.* **2015,** *137* (37), 12143-12152.
9. Jin, Z.-Q.; Liu, Y.-G.; Wang, W.-K.; Wang, A.-B.; Hu, B.-W.; Shen, M.; Gao, T.; Zhao, P.-C.; Yang, Y.-S., A New Insight Into the Lithium Storage Mechanism of Sulfurized Polyacrylonitrile with No Soluble Intermediates. *Energy Storage Materials* **2018,** *14*, 272-278.
10. Wang, X.; Qian, Y.; Wang, L.; Yang, H.; Li, H.; Zhao, Y.; Liu, T., Sulfurized Polyacrylonitrile Cathodes with High Compatibility in Both Ether and Carbonate Electrolytes for Ultrastable Lithium–Sulfur Batteries. *Adv. Funct. Mater.* **2019,** *29* (39), Article no. 1902929.
11. Fan, L.; Chen, S.; Zhu, J.; Ma, R.; Li, S.; Podila, R.; Rao, A. M.; Yang, G.; Wang, C.; Liu, Q.; Xu, Z.; Yuan, L.; Huang, Y.; Lu, B., Simultaneous Suppression of the Dendrite Formation and Shuttle Effect in a Lithium–Sulfur Battery by Bilateral Solid Electrolyte Interface. *Advanced Science* **2018,** *5* (9), 1700934.
12. Yang, H.; Chen, J.; Yang, J.; Wang, J., Prospect of Sulfurized Pyrolyzed Poly(acrylonitrile) (S@pPAN) Cathode Materials for Rechargeable Lithium Batteries. *Angew. Chem., Int. Ed.* **2020,** *59* (19), 7306-7318.
13. Zhang, S., Understanding of Sulfurized Polyacrylonitrile for Superior Performance Lithium/Sulfur Battery. *Energies* **2014,** *7* (7), 4588-4600.
14. Lee, J. T.; Eom, K.; Wu, F.; Kim, H.; Lee, D. C.; Zdyrko, B.; Yushin, G., Enhancing the Stability of Sulfur Cathodes in Li–S Cells via in Situ Formation of a Solid Electrolyte Layer. *ACS Energy Lett.* **2016,** *1* (2), 373-379.

15. Wang, L.; Ye, Y.; Chen, N.; Huang, Y.; Li, L.; Wu, F.; Chen, R., Development and Challenges of Functional Electrolytes for High-Performance Lithium–Sulfur Batteries. *Adv. Funct. Mater.* **2018,** *28* (38), 1800919.
16. Camacho-Forero, L. E.; Smith, T. W.; Bertolini, S.; Balbuena, P. B., Reactivity at the Lithium–Metal Anode Surface of Lithium–Sulfur Batteries. *The Journal of Physical Chemistry C* **2015,** *119* (48), 26828-26839.
17. Warneke, S.; Hintennach, A.; Buchmeiser, M. R., Communication—Influence of Carbonate-Based Electrolyte Composition on Cell Performance of SPAN-Based Lithium-Sulfur-Batteries. *J. Electrochem. Soc.* **2018,** *165* (10), A2093-A2095.
18. Shkrob, I. A.; Wishart, J. F.; Abraham, D. P., What Makes Fluoroethylene Carbonate Different? *J. Phys. Chem. C* **2015,** *119* (27), 14954-14964.
19. Markevich, E.; Salitra, G.; Rosenman, A.; Talyosef, Y.; Chesneau, F.; Aurbach, D., The Effect of a Solid Electrolyte Interphase on the Mechanism of Operation of Lithium–Sulfur Batteries. *J. Mater. Chem. A* **2015,** *3* (39), 19873-19883.
20. Leung, K.; Rempe, S. B.; Foster, M. E.; Ma, Y.; Martinez del la Hoz, J. M.; Sai, N.; Balbuena, P. B., Modeling Electrochemical Decomposition of Fluoroethylene Carbonate on Silicon Anode Surfaces in Lithium Ion Batteries. *J. Electrochem. Soc.* **2013,** *161* (3), A213-A221.
21. Wang, X.; Tan, Y.; Shen, G.; Zhang, S., Recent Progress in Fluorinated Electrolytes for Improving the Performance of Li–S Batteries. *J. Energy Chem.* **2020,** *41*, 149-170.
22. Wang, Y.; Nakamura, S.; Ue, M.; Balbuena, P. B., Theoretical Studies To Understand Surface Chemistry on Carbon Anodes for Lithium-Ion Batteries: Reduction Mechanisms of Ethylene Carbonate. *J. Am. Chem. Soc.* **2001,** *123* (47), 11708-11718.
23. Xu, K., Nonaqueous Liquid Electrolytes for Lithium-Based Rechargeable Batteries. *Chem. Rev.* **2004,** *104* (10), 4303-4418.
24. Markevich, E.; Salitra, G.; Talyosef, Y.; Chesneau, F.; Aurbach, D., Review—On the Mechanism of Quasi-Solid-State Lithiation of Sulfur Encapsulated in Microporous Carbons: Is the Existence of Small Sulfur Molecules Necessary? *J. Electrochem. Soc.* **2017,** *164* (1), A6244-A6253.
25. Xue, W.; Shi, Z.; Huang, M.; Feng, S.; Wang, C.; Wang, F.; Lopez, J.; Qiao, B.; Xu, G.; Zhang, W.; Dong, Y.; Gao, R.; Shao-Horn, Y.; Johnson, J. A.; Li, J., FSI-inspired solvent and “full fluorosulfonyl” electrolyte for 4 V class lithium-metal batteries. *Energy Environ. Sci.* **2020,** *13* (1), 212-220.
26. Shkrob, I. A.; Marin, T. W.; Zhu, Y.; Abraham, D. P., Why Bis(fluorosulfonyl)imide Is a “Magic Anion” for Electrochemistry. *J. Phys. Chem. C* **2014,** *118* (34), 19661-19671.
27. Kresse, G.; Hafner, J., Ab Initio Molecular-Dynamics Simulation of the Liquid-Metal--Amorphous-Semiconductor Transition in Germanium. *Phys. Rev. B* **1994,** *49* (20), 14251-14269.
28. Kresse, G.; Furthmüller, J., Efficient Iterative Schemes for Ab Initio Total-Energy Calculations Using a Plane-Wave Basis Set. *Phys. Rev. B* **1996,** *54* (16), 11169-11186.
29. Kresse, G.; Furthmuller, J., Efficiency of ab-initio total energy calculations for metals and semiconductors using a plane-wave basis set. *Comput. Mater. Sci.* **1996,** *6* (1), 15-50.
30. Takahashi, T.; Yamagata, M.; Ishikawa, M., A Sulfur–Microporous Carbon Composite Positive Electrode for Lithium/Sulfur and Silicon/Sulfur Rechargeble Batteries. *Progress in Natural Science: Materials International* **2015,** *25* (6), 612-621.
31. Azimi, N.; Xue, Z.; Rago, N. D.; Takoudis, C.; Gordin, M. L.; Song, J.; Wang, D.; Zhang, Z., Fluorinated Electrolytes for Li-S Battery: Suppressing the Self-Discharge with an Electrolyte Containing Fluoroether Solvent. *Journal of The Electrochemical Society* **2014,** *162* (1), A64-A68.
32. Kresse, G.; Joubert, D., From Ultrasoft Pseudopotentials to the Projector Augmented-Wave Method. *Phys. Rev. B* **1999,** *59* (3), 1758-1775.

33. Perdew, J. P.; Burke, K.; Ernzerhof, M., Generalized Gradient Approximation Made Simple. *Phys. Rev. Lett.* **1996,** *77* (18), 3865-3868.
34. Monkhorst, H. J.; Pack, J. D., Special Points for Brillouin-Zone Integrations. *Phys. Rev. B* **1976,** *13* (12), 5188-5192.
35. Grimme, S.; Antony, J.; Ehrlich, S.; Krieg, H., A Consistent and Accurate Ab Initio Parametrization of Density Functional Dispersion Correction (DFT-D) for the 94 Elements H-Pu. *J. Chem. Phys.* **2010,** *132* (15), Article no. 154104.
36. Dysart, A. D.; Burgos, J. C.; Mistry, A.; Chen, C.-F.; Liu, Z.; Hong, C. N.; Balbuena, P. B.; Mukherjee, P. P.; Pol, V. G., Towards Next Generation Lithium-Sulfur Batteries: Non-Conventional Carbon Compartments/Sulfur Electrodes and Multi-Scale Analysis. *Journal of The Electrochemical Society* **2016,** *163* (5), A730-A741.
37. Burgos, J. C.; Balbuena, P. B.; Montoya, J. A., Structural Dependence of the Sulfur Reduction Mechanism in Carbon-Based Cathodes for Lithium–Sulfur Batteries. *The Journal of Physical Chemistry C* **2017,** *121* (34), 18369-18377.
38. Zhang, Q.; Wang, Y.; Seh, Z. W.; Fu, Z.; Zhang, R.; Cui, Y., Understanding the Anchoring Effect of Two-Dimensional Layered Materials for Lithium–Sulfur Batteries. *Nano Letters* **2015,** *15* (6), 3780-3786.
39. Maintz, S.; Deringer, V. L.; Tchougréeff, A. L.; Dronskowski, R., LOBSTER: A tool to Extract Chemical Bonding From Plane-Wave Based DFT. *J. Comput. Chem.* **2016,** *37* (11), 1030-1035.
40. Nelson, R.; Ertural, C.; George, J.; Deringer, V. L.; Hautier, G.; Dronskowski, R., LOBSTER: Local Orbital Projections, Atomic Charges, and Chemical-Bonding Analysis from Projector-Augmented-Wave-Based Density-Functional Theory. *J. Comput. Chem.* **2020,** *41* (21), 1931-1940.
41. Tang, W.; Sanville, E.; Henkelman, G., A Grid-Based Bader Analysis Algorithm Without Lattice Bias. *J. Phys.: Condens. Matter* **2009,** *21* (8), Article no. 084204.
42. Sun, H.; Mumby, S. J.; Maple, J. R.; Hagler, A. T., An Ab Initio CFF93 All-Atom Force Field for Polycarbonates. *J. Am. Chem. Soc.* **1994,** *116* (7), 2978-2987.
43. Borodin, O.; Gorecki, W.; Smith, G. D.; Armand, M., Molecular Dynamics Simulation and Pulsed-Field Gradient NMR Studies of Bis(fluorosulfonyl)imide (FSI) and Bis[(trifluoromethyl)sulfonyl]imide (TFSI)-Based Ionic Liquids. *J. Phys. Chem. B* **2010,** *114* (20), 6786-6798.
44. Canongia Lopes, J. N.; Shimizu, K.; Pádua, A. A. H.; Umebayashi, Y.; Fukuda, S.; Fujii, K.; Ishiguro, S.-i., Potential Energy Landscape of Bis(fluorosulfonyl)amide. *J. Phys. Chem. B* **2008,** *112* (31), 9449-9455.
45. Yamada, Y.; Yamada, A., Review—Superconcentrated Electrolytes for Lithium Batteries. *J. Electrochem. Soc.* **2015,** *162* (14), A2406-A2423.
46. Perez Beltran, S.; Balbuena, P. B., Sulfurized Polyacrylonitrile for High-Performance Lithium–Sulfur Batteries: In-Depth Computational Approach Revealing Multiple Sulfur's Reduction Pathways and Hidden Li+ Storage Mechanisms for Extra Discharge Capacity. *ACS Appl. Mater. Interfaces* **2021,** *13* (1), 491-502.
47. Wang, L.; He, X.; Li, J.; Chen, M.; Gao, J.; Jiang, C., Charge/Discharge Characteristics of Sulfurized Polyacrylonitrile Composite with Different Sulfur Content in Carbonate Based Electrolyte for Lithium Batteries. *Electrochim. Acta* **2012,** *72*, 114-119.
48. Fanous, J.; Wegner, M.; Spera, M. B. M.; Buchmeiser, M. R., High Energy Density Poly(acrylonitrile)-Sulfur Composite-Based Lithium-Sulfur Batteries. *J. Electrochem. Soc.* **2013,** *160* (8), A1169-A1170.
49. Frey, M.; Zenn, R. K.; Warneke, S.; Müller, K.; Hintennach, A.; Dinnebier, R. E.; Buchmeiser, M. R., Easily Accessible, Textile Fiber-Based Sulfurized Poly(acrylonitrile) as Li/S Cathode Material: Correlating Electrochemical Performance with Morphology and Structure. *ACS Energy Lett.* **2017,** *2* (3), 595-604.

50. Otani, M.; Sugino, O., First-Principles Calculations of Charged Surfaces and Interfaces: A Plane-Wave Nonrepeated Slab Approach. *Phys. Rev. B* **2006,** *73* (11), 115407.
51. Haruyama, J.; Ikeshoji, T.; Otani, M., Analysis of Lithium Insertion/Desorption Reaction at Interfaces between Graphite Electrodes and Electrolyte Solution Using Density Functional + Implicit Solvation Theory. *J. Phys. Chem. C* **2018,** *122* (18), 9804-9810.
52. Han, J.; Zheng, Y.; Guo, N.; Balbuena, P. B., Calculated Reduction Potentials of Electrolyte Species in Lithium-Sulfur Batteries. *J. Phys. Chem. C* **2020**.
53. Zhang, S. S., Liquid Electrolyte Lithium/Sulfur Battery: Fundamental Chemistry, Problems, and Solutions. *J. Power Sources* **2013,** *231*, 153-162.
54. Yang, H.; Naveed, A.; Li, Q.; Guo, C.; Chen, J.; Lei, J.; Yang, J.; Nuli, Y.; Wang, J., Lithium Sulfur Batteries with Compatible Electrolyte both for Stable Cathode and Dendrite-Free Anode. *Energy Storage Materials* **2018,** *15*, 299-307.
55. He, X.; Pu, W.; Ren, J.; Wang, L.; Wang, J.; Jiang, C.; Wan, C., Charge/Discharge Characteristics of Sulfur Composite Cathode Materials in Rechargeable Lithium Batteries. *Electrochim. Acta* **2007,** *52* (25), 7372-7376.
56. Martinez de la Hoz, J. M.; Leung, K.; Balbuena, P. B., Reduction Mechanisms of Ethylene Carbonate on Si Anodes of Lithium-Ion Batteries: Effects of Degree of Lithiation and Nature of Exposed Surface. *ACS Appl. Mater.* **2013,** *5* (24), 13457-13465.
57. Markevich, E.; Salitra, G.; Fridman, K.; Sharabi, R.; Gershinsky, G.; Garsuch, A.; Semrau, G.; Schmidt, M. A.; Aurbach, D., Fluoroethylene Carbonate as an Important Component in Electrolyte Solutions for High-Voltage Lithium Batteries: Role of Surface Chemistry on the Cathode. *Langmuir* **2014,** *30* (25), 7414-7424.
58. Leung, K.; Budzien, J. L., Ab Initio Molecular Dynamics Simulations of the Initial Stages of Solid–Electrolyte Interphase Formation on Lithium Ion Battery Graphitic Anodes. *Phys. Chem. Chem. Phys.* **2010,** *12* (25), 6583-6586.
59. Yu, J.; Balbuena, P. B.; Budzien, J.; Leung, K., Hybrid DFT Functional-Based Static and Molecular Dynamics Studies of Excess Electron in Liquid Ethylene Carbonate. *J. Electrochem. Soc.* **2011,** *158* (4), A400.
60. Borodin, O.; Ren, X.; Vatamanu, J.; von Wald Cresce, A.; Knap, J.; Xu, K., Modeling Insight into Battery Electrolyte Electrochemical Stability and Interfacial Structure. *Accounts of Chemical Research* **2017,** *50* (12), 2886-2894.
61. Xu, K., Electrolytes and Interphases in Li-Ion Batteries and Beyond. *Chem. Rev.* **2014,** *114* (23), 11503-11618.
62. Islam, M. M.; Ostadhossein, A.; Borodin, O.; Yeates, A. T.; Tipton, W. W.; Hennig, R. G.; Kumar, N.; van Duin, A. C. T., ReaxFF Molecular Dynamics Simulations on Lithiated Sulfur Cathode Materials. *Phys. Chem. Chem. Phys.* **2015,** *17* (5), 3383-3393.
63. Etacheri, V.; Haik, O.; Goffer, Y.; Roberts, G. A.; Stefan, I. C.; Fasching, R.; Aurbach, D., Effect of Fluoroethylene Carbonate (FEC) on the Performance and Surface Chemistry of Si-Nanowire Li-Ion Battery Anodes. *Langmuir* **2012,** *28* (1), 965-976.
64. Martínez de la Hoz, J. M.; Balbuena, P. B., Reduction Mechanisms of Additives on Si Anodes of Li-ion Batteries. *Phys. Chem. Chem. Phys.* **2014,** *16* (32), 17091-17098.
65. Philippe, B.; Dedryvère, R.; Gorgoi, M.; Rensmo, H.; Gonbeau, D.; Edström, K., Role of the LiPF6 Salt for the Long-Term Stability of Silicon Electrodes in Li-Ion Batteries – A Photoelectron Spectroscopy Study. *Chem. Mater.* **2013,** *25* (3), 394-404.
66. Suo, L.; Xue, W.; Gobet, M.; Greenbaum, S. G.; Wang, C.; Chen, Y.; Yang, W.; Li, Y.; Li, J., Fluorine-Donating Electrolytes Enable Highly Reversible 5-V-Class Li Metal Batteries. *Proceedings of the National Academy of Sciences* **2018,** *115* (6), 1156-1161.
67. Ohwaki, T.; Ozaki, T.; Okuno, Y.; Ikeshoji, T.; Imai, H.; Otani, M., Li Deposition and Desolvation with Electron Transfer at a Silicon/Propylene-Carbonate Interface: Transition-State and Free-Energy Profiles by Large-Scale First-Principles Molecular Dynamics. *Phys. Chem. Chem. Phys.* **2018,** *20* (17), 11586-11591.

68. Leung, K., Two-Electron Reduction of Ethylene Carbonate: A Quantum Chemistry Re-Examination of Mechanisms. *Chemical Physics Letters* **2013,** *568-569*, 1-8.
69. Budi, A.; Basile, A.; Opletal, G.; Hollenkamp, A. F.; Best, A. S.; Rees, R. J.; Bhatt, A. I.; O'Mullane, A. P.; Russo, S. P., Study of the Initial Stage of Solid Electrolyte Interphase Formation upon Chemical Reaction of Lithium Metal and N-Methyl-N-Propyl-Pyrrolidinium-Bis(Fluorosulfonyl)Imide. *J. Phys. Chem. C* **2012,** *116* (37), 19789-19797.
70. Ospina Acevedo, F.; Guo, N.; Balbuena, P. B., Lithium Oxidation and Electrolyte Decomposition at Li-Metal/Liquid Electrolyte Interfaces. *J.Mater. Chem. A* **2020,** *8*, 17036-17055.
71. Perez Beltran, S.; Cao, X.; Zhang, J.-G.; Balbuena, P. B., Localized High Concentration Electrolytes for High Voltage Lithium–Metal Batteries: Correlation between the Electrolyte Composition and Its Reductive/Oxidative Stability. *Chem. Mater.* **2020,** *32* (14), 5973-5984.